

## Simulation of Deformation and Fracture Characteristics of a 45 Steel Taylor Impact Specimen

Gang CHEN, Xicheng HUANG

*Institute of Systems Engineering*  
*Chinese Academy of Engineering Physics*  
Sichuan, China, 621999  
e-mail: {chengang, huangxc}@caep.cn

The Taylor impact test was originally developed as a method for estimating the dynamic strength of ductile materials at high strain rates. More recently, the Taylor test has been used to verify material constitutive models by comparing numerical predictions with experimental data, since it provides a wide range of plastic strains and strain rates in various stress states. When the impact velocity is sufficiently high, a specimen will generate cracks in the Taylor test. Only few studies investigated so far the fracture phenomena and mechanisms in the Taylor test. In this paper, based on investigation of material dynamic behaviour, the deformation and fracture characteristics of a 45 steel specimen under Taylor impact test were simulated using axial symmetry and three-dimensional model was developed with LS-DYNA software. The final length and diameter of the specimen, obtained in simulations, were consistent with the experimental observations. Different dynamic fractures that occurred in the Taylor test were obtained in three-dimensional numerical simulations as well. The mechanisms of different failure modes were investigated using the history of stress state triaxiality of the specimen.

**Key words:** Taylor impact, numerical simulation, 45 steel, fracture.

### 1. INTRODUCTION

The Taylor test was developed by G.I. Taylor as a method of estimating the dynamic strength of ductile materials under compression. This test consists of firing a flat-nosed cylindrical projectile made of a ductile material onto a massive and rigid target at normal incidence. The dynamic flow stress can be estimated by measuring the dimensions of a cylinder before and after deformation.

The analytical analysis of the Taylor test gained importance in the past, in spite of the fact that it was one-dimensional. However, it is clear that material moves in three- dimensions during the Taylor impact test. In addition, the

strain rate during the deformation process is not constant. On the opposite, the strain in the deformation range varies at different places. Nowadays, with the development of numerical simulation techniques, the Taylor test has been used by a number of researchers [1–5] to validate constitutive strength models by correlating final cylinder shape of experimental test and numerical simulation result. In addition, some researchers used the Taylor impact test to evaluate constitutive models and to determine constants for these models [6–8].

Most of the studies involving the Taylor test focus on determining the dynamic yield stress and constitutive models of materials without considering fracture characteristics. If the impact velocity during the test is sufficiently high, failure will occur and cracks will be generated in a cylinder. Until now, few published papers have dealt with fracture phenomena and fracture mechanisms in the Taylor test.

Two types of fracture behaviour were observed in the Taylor tests performed by PAPIRNO *et al.* with 4340 steel in different heat treatment conditions [9]. One type was brittle fracture with a conical fracture surface at the impact end of the projectile. The other type involved fracture, where the impact surface petals while the projectile remains intact [9]. GRADY and KIPP [10] found large number of void nucleation, growth and aggregation in the centre of specimen near the impact interface. The similar experimental phenomena were also reported by WOODWARD in [11]. The dynamic fracture behaviours of Ti-6Al-4V alloy at high strain rate loading were investigated using the Taylor impact test in [12], where the critical impact velocity and microscopic analyses of fracture surface were given. The deformation and failure behaviour of flat projectiles manufactured from 7A04-T6 aluminium alloy were investigated in [13], where three deformation and failure modes, i.e., mushrooming, shear cracking and fragmentation were observed, while the impact velocity increased. Taylor bar impact tests were conducted by RAKVÅG *et al.* in [14] using tool steel projectiles with three different values of hardness at impact velocity ranging from 100 to 350 m/s. In their study, several different deformation and fracture modes were registered for each hardness value. Taylor impact tests in the classic and symmetric configurations were applied to analyse the development of plastic deformation and damage in Al-6082-T6 rods and internal axial damage was identified using metallography in [15].

In fact, the fracture and fragmentation in the Taylor impact does not maintain axisymmetric characteristic, and this phenomena need to be described with a three-dimensional (3D) model. Still, numerical prediction of crack growth and fracture in a 3D body under multi-axial dynamic loading is a challenging problem. Three possible fracture modes in the Taylor impact: the confined fracture inside the cylinder, the shear cracking on the lateral surface, and the

petalling, were simulated by TENG *et al.* in [16]. However, the authors did not provide direct comparison with experimental data for all three modes. Three deformation and failure modes of penetration mechanisms, i.e., Taylor mushrooming, sunflower-like petalling and plugging perforation were observed in the experiments and corresponding simulations of A3 steel blunt projectiles impacting 45 steel plates by CHEN [17]. A numerical study on the deformation and fracture modes of steel projectiles during Taylor bar impact tests described in [14] was carried out in [18], where fracture modes and critical velocities observed in experimental tests were reproduced in numerical simulations.

In this paper, based on investigation of material dynamic behaviours, the dynamic deformation and failure of 45 steel in Taylor cylindrical impact test were investigated using LS-DYNA software that provided the dynamic finite element simulation. The mechanisms of different failure modes were investigated with obtained simulation results.

## 2. MATERIAL BEHAVIOURS AND MODEL DESCRIPTION

In the numerical simulation of dynamics, material constitutive models must be able to depict exactly material behaviours under conditions of large strain and wide range of strain rates and temperatures. The Johnson-Cook (JC) model is often used to study the dynamic behaviours of metals, ranging from low to high strain rates, and it is appropriate to study the quasi-static deformation too. The JC model was chosen in this study to describe the plastic behaviour and failure property of 45 steel material. The JC model consists of two parts. The first part [1] describes material plastic flow stress that varies with strain, strain rate and temperature, and is as follows:

$$(2.1) \quad \sigma_{eq} = [A + B(\bar{\epsilon}^p)^n][1 + C \ln \dot{\epsilon}^*][1 - (T^*)^m],$$

where  $A$ ,  $B$ ,  $C$ ,  $n$  and  $m$  are material constants,  $\dot{\epsilon}^* = \dot{\bar{\epsilon}}^p / \dot{\epsilon}_0$  is a dimensionless strain rate,  $\dot{\epsilon}_0$  is a reference strain rate, and  $T^* = (T - T_r) / (T_m - T_r)$  is the homologous temperature, where  $T$  is the absolute temperature,  $T_r$  is the room temperature and  $T_m$  is the material melting temperature.

The second part [19] describes material failure with a damage parameter  $D$  which is

$$(2.2) \quad D = \sum \frac{\Delta \epsilon_p}{\epsilon^f},$$

where  $\Delta \epsilon_p$  is the increment of effective plastic strain during an integration cycle and  $\epsilon^f$  is the equivalent strain to failure, under the current conditions of strain,

temperature, pressure and equivalent stress. Failure is allowed to occur when  $D = 1.0$ . The general expression for the strain at fracture is given by

$$(2.3) \quad \varepsilon^f = [D_1 + D_2 \exp(D_3 \sigma^*)][1 + D_4 \ln \dot{\varepsilon}^*][1 + D_5 T^*],$$

where  $\sigma^* = -R^\sigma = p/\sigma_{eq}$  is the stress triaxiality ratio and  $p$  is pressure. The parameters  $D_1$ ,  $D_2$ ,  $D_3$ ,  $D_4$  and  $D_5$  are material constants. The failure strain and thus the accumulation of damage is a function of mean stress, strain rate and temperature.

In the absence of significant heat conduction at rare times, a higher velocity impact is usually regarded as under adiabatic condition. The majority of plastic energy is converted into heat and this generates localised high temperature. The adiabatic temperature rise can be expressed as

$$(2.4) \quad \Delta T = \frac{\eta}{\rho C_p} \int_0^\varepsilon \sigma(\varepsilon_p) d\varepsilon_p,$$

where  $C_p$  is the specific heat,  $\eta$  is the fraction of plastic work converted into heat and  $\rho$  is the material density.

Dynamic and quasi-static mechanical behaviour of 45 steel was studied in [20] using the split Hopkinson pressure bar (SHPB) and static material test system over a wide range of strain rates and temperatures. The experimental results are given in Figs. 1 and 2.

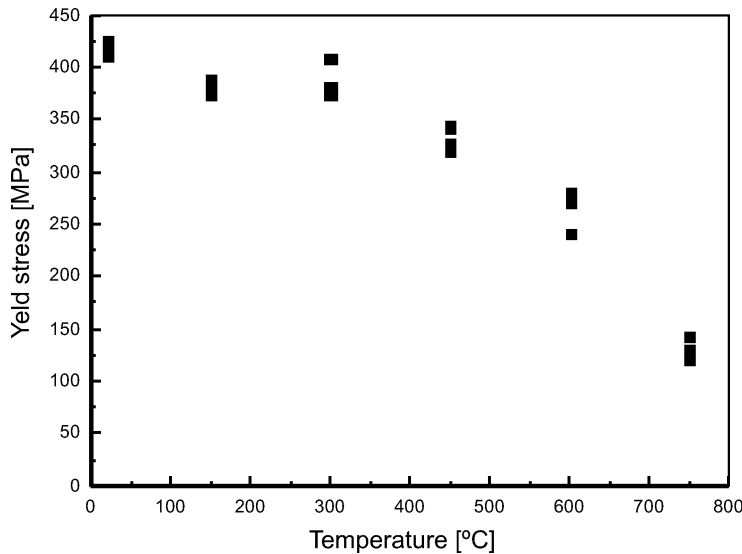


FIG. 1. Tensional yield stress of 45 steel vs. temperature.

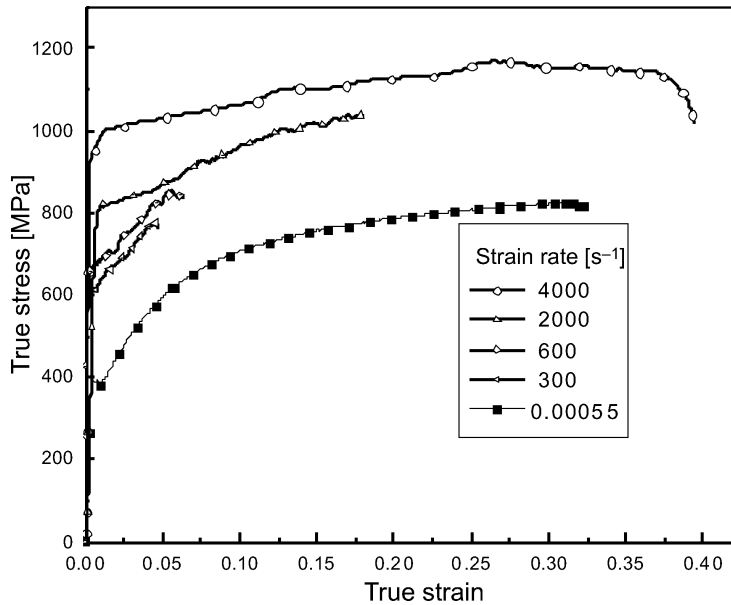


FIG. 2. Compressive stress – strain curves of 45 steel at different strain rates.

The effects of high strain rate, elevated temperature and stress triaxiality on the fracture behaviour of 45 steel were studied in [21] using split Hopkinson tension bar tests and static material test. The quasi-static experiments of compressive, torsional, and tensile of both smooth and notched specimen were conducted to study the effects of stress triaxiality. Tensile experiments at different strain-rates and elevated temperatures were conducted to study the effects of strain-rate and temperature. Failure strain of 45 steel vs. stress triaxiality, temperature and strain rate in various cases of experiments are shown in Figs. 3–5,

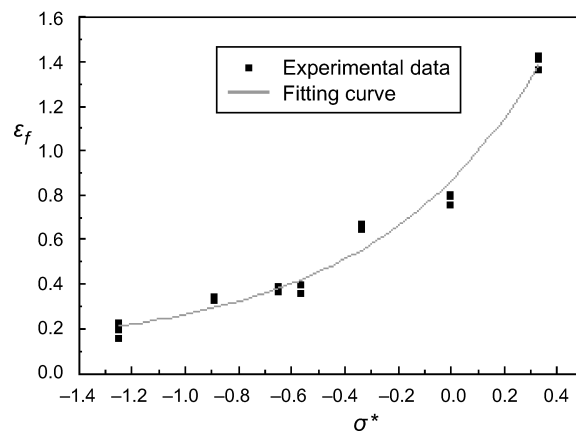


FIG. 3. Failure strain of 45 steel vs. stress triaxiality.

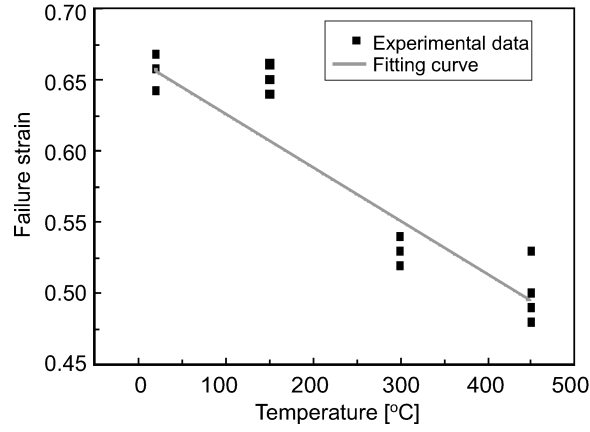


FIG. 4. Tension failure strain of 45 steel vs. temperature.

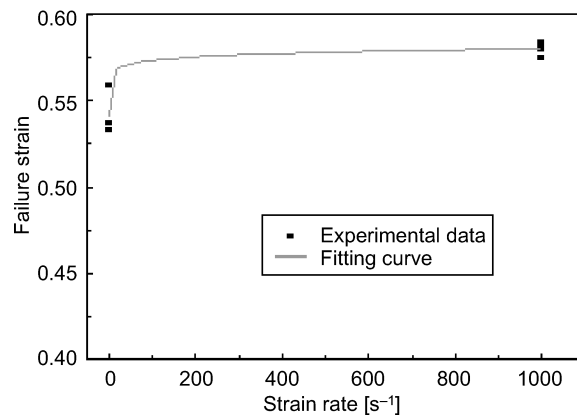


FIG. 5. Failure strain of 45 steel vs. strain rate.

respectively. The failure strain increased markedly with stress triaxiality, slightly decreased with temperature, and slightly increased with strain rate.

Based on material property experiments shown above and with the method of least squares, the parameters used in this simulation were obtained and they are shown in Table 1 (the reference strain rate is  $1 \text{ s}^{-1}$ ).

**Table 1.** Material parameters of 45 steel.

P [kg/m <sup>3</sup> ]	E[GPa]	$\mu$	$C_p$ [W/(m · K)]	$\eta$	$T_r$ [K]	$T_m$ [K]	$\dot{\epsilon}_0$ [s <sup>-1</sup> ]	A[MPa]	B [MPa]
7800	200	0.3	469	1	300	1795	1	506	320
$n$	$C$	$m$	$D_1$	$D_2$	$D_3$	$D_4$	$D_5$		
0.28	0.064	1.06	0.1	0.76	1.57	0.005	-0.84		

## 3. ON THE TAYLOR IMPACT DEFORMATION

The deformation responses of Taylor impact specimen under different impacting speeds were simulated with axisymmetric model using LS-DYNA. The axisymmetric model was established according to the experimental conditions, as shown in Fig. 6. The mesh scale of specimen was  $0.5 \times 0.5$  mm. The target was described with elastic material model, and the specimen material was described with the JC model as mentioned earlier. The interaction of the specimen with the target was defined by the dynamic contact algorithm.

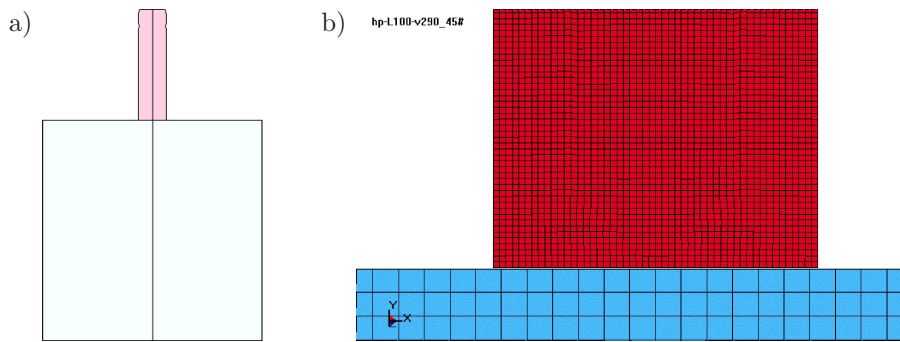


FIG. 6. Axisymmetric FEM model for Taylor impact: a) global, b) local mesh.

The simulation results of the final deformation and the equivalent plastic strain distribution of a 45 steel Taylor impact specimen in the cases of impact velocity of 164 m/s, 217 m/s and 290 m/s are given in Fig. 7. The distribution

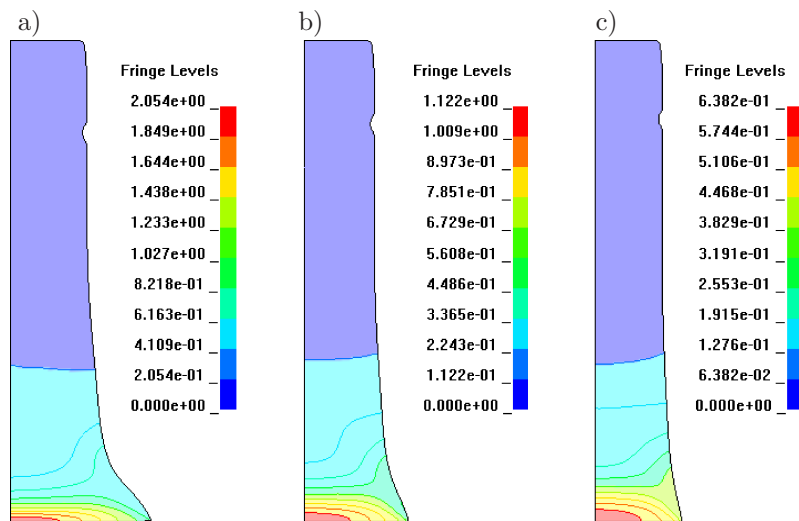


FIG. 7. The final deformation of a specimen at different impact velocities:  
a) 164 m/s, b) 217 m/s, c) 290 m/s.

of plastic strain in the specimen is non-uniform (either in radial or axial direction), the maximum plastic strain is located at the centre of the impact section, and its values under these three velocities are 0.64, 1.1 and 2.1, respectively. A comparison of specimen shapes obtained in the experiment and the numerical simulation is given in Fig. 8. The comparison of the final length and the maximum diameter of specimen is given in Fig. 9. The consistency between experimental observations and numerical simulations indicates that the obtained

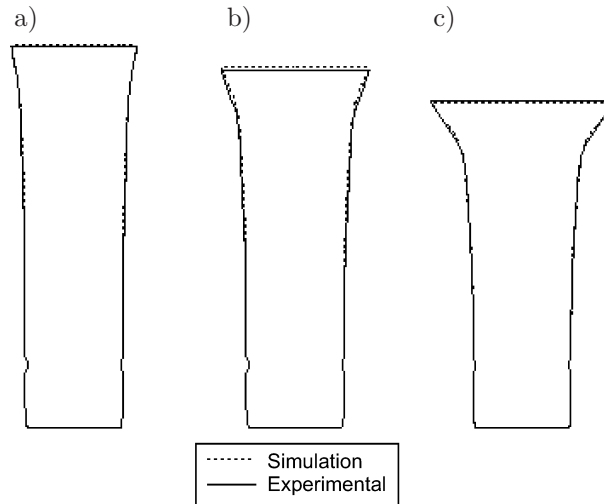


FIG. 8. Comparison of a specimen final shapes between simulation and experiment: a) 164 m/s, b) 217 m/s, c) 290 m/s.

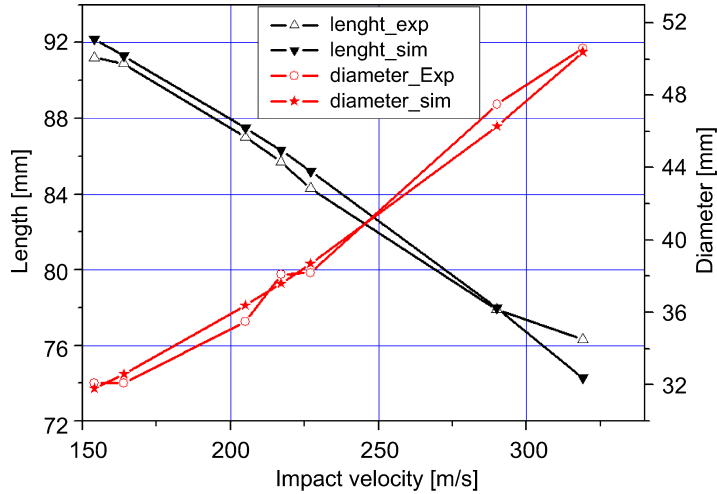


FIG. 9. Comparison of a specimen final length and maximum diameter between simulation and experiment.

material parameters can describe the large strain mechanical behaviour of 45 steel under high speed deformation.

The loading history curves at three impact velocities obtained in our simulation are given in Fig. 10. All the curves have similar characteristics. A high peak value arose at the early stage of the impact process, and its amplitude was approximately proportional to the impact velocity. The loads, then, reduced to a lower level in 10  $\mu$ s and maintained at a platform, the amplitude of the plate increased slightly with initial velocity and varied at the range of 90 kN to 150 kN. Then, the impact loads decreased slowly at the end of collision after 80  $\mu$ s. The interaction duration between the specimen and the target increased slightly with the impact velocity. The loading curves reflected the mechanical state of the specimen material at the process of impact as following: the material near the impact interface was almost in the state of plane strain during the initial stage, and the impact load was mainly the function of velocity. At the following stage, the loading platform reflected the stress characteristics of material steady plastic deformation state.

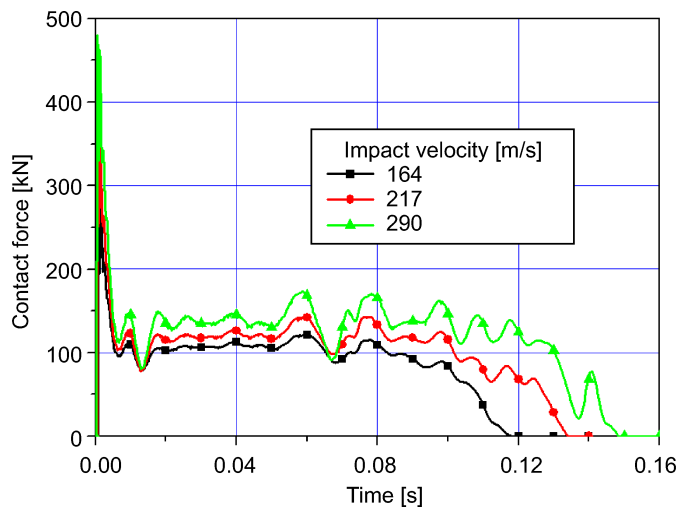


FIG. 10. The loading history curves at three impact velocities.

The specimen rigid-body velocity histories of several simulation cases are given in Fig. 5. The specimen bounced velocity was about 19 m/s at impact velocity varying from 154 m/s to 227 m/s, while it was 12 m/s at impact velocity of 319 m/s. This is because of high temperature, during high speed impact, generated by large plastic deformation at the impact end of the specimen, which causes material softening. This softening causes a decrease in bounce velocity.

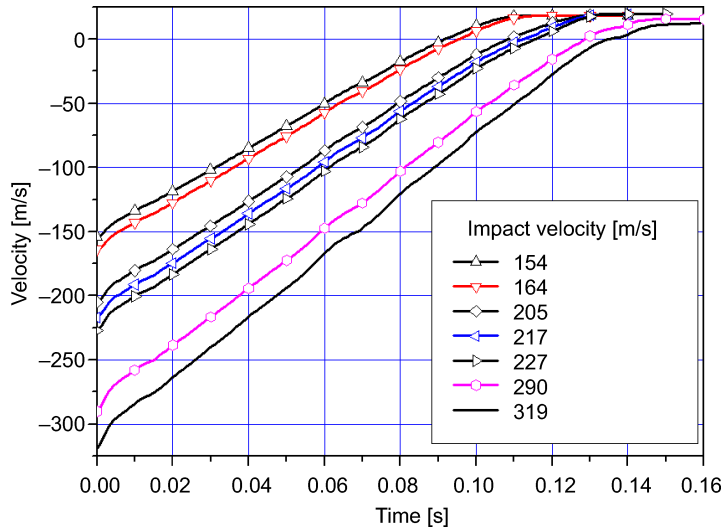


FIG. 11. Rigid-body velocity histories at several impact velocity cases.

Figures 12 and 13 show equivalent plastic strain histories and stress triaxiality histories of three elements at the specimen impact end in the case of the initial impact velocity of 217 m/s, respectively. The three elements are located at: impact end centre of the specimen, edge of the specimen and the middle point between the other two elements. From these figures, it can be seen that,

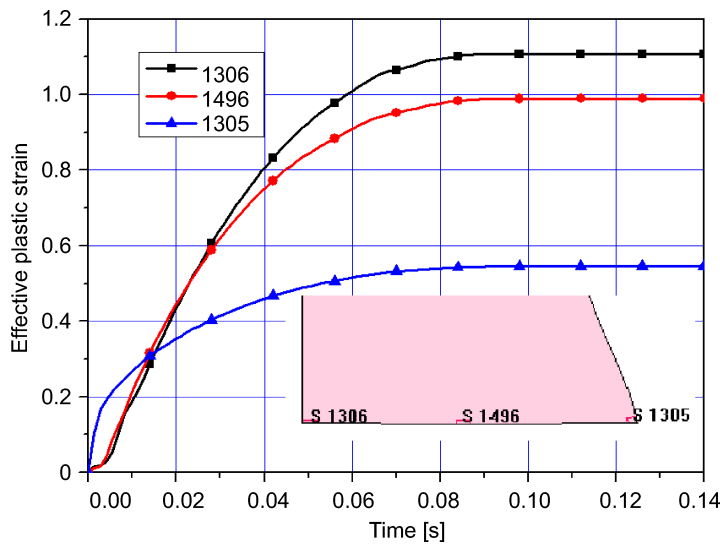


FIG. 12. Plastic strain histories of three elements at the specimen impact end (217 m/s).

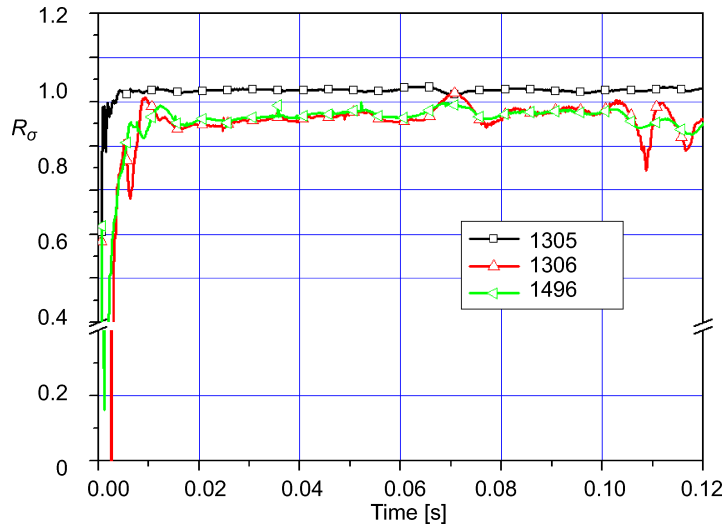


FIG. 13. Stress state triaxiality histories of three elements at the specimen impact end (217 m/s).

at the initial stage of impact, all the elements were subjected to compressive loadings, and the strain of the edge element was growing faster than that of the central part. After the first stage, the strain growth at the edge became slow, and the strain growth was maintained at the central part. Finally, at the end of impact, the plastic strain at the central part was larger than the one at the edge.

Figure 13 shows that the stress triaxiality of the element at the edge is negative in the first 5  $\mu\text{s}$  of the impact. This indicates that the stress state is compressive at that moment, and after that, the triaxiality changes to positive, which indicates that the stress state of the edge is tensile. While at the central part, the stress triaxiality is negative during the whole impacting process, that is, the material is always subjected to compressive loading. Therefore, in consideration of the relationship of material failure strain and stress triaxiality, the material fracture may occur first at the edge even if the strain at the centre part is much larger.

#### 4. ON THE SPECIMEN FAILURE UNDER TAYLOR IMPACT

Although the experimental design of Taylor impact can be considered to be axisymmetric, the failure of a specimen is not symmetric. Thus, simple axisymmetric finite element modelling (FEM) is unable to simulate the failure. A 3D solid element was employed to model both the specimen and the target.

The technique of element deletion was used to simulate erosion of the specimen. When the accumulative damage of an element exceeded the critical value, all the components of stress in the element were set to zero, the material failed, and the element was deleted in the subsequent calculation. To reduce the influence of element deletion on the structural impact, one has to minimise the mesh size of FEM, within the allowable computational time. In the simulation, the specimen element size was modelled as  $0.45 \times 0.45 \times 1.25$  mm, in which the longest edge is along the axial direction.

The specimen deformation and damage distribution for impact velocities of 217 m/s, 290 m/s, 319 m/s and 350 m/s are given in Fig. 14. In the case of 217 m/s, the maximum damage was 0.6, and there was no failure in specimen, but the maximum damage appeared at the edge of impact end. In the case of 290 m/s, a crack failure appeared at the edge of the impact end, which is

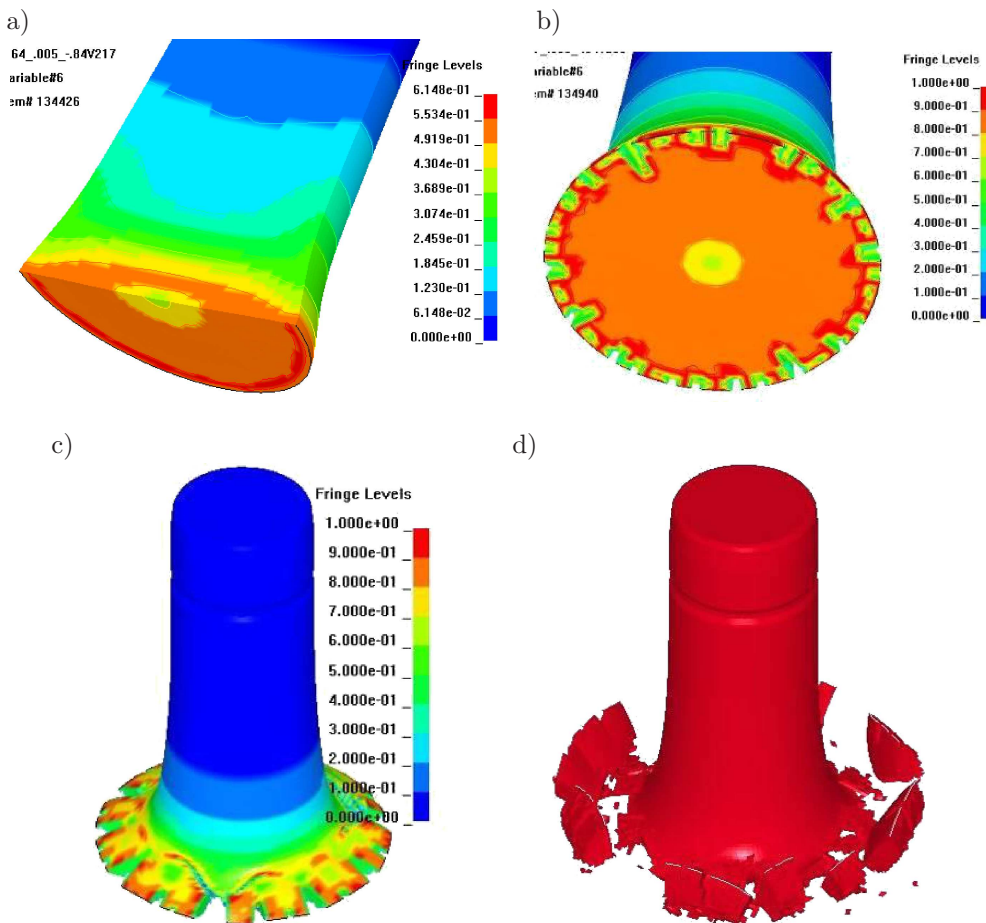


FIG. 14. The specimen deformation and damage for different impact velocities:  
a) 217 m/s, b) 290 m/s, c) 319 m/s, d) 350 m/s.

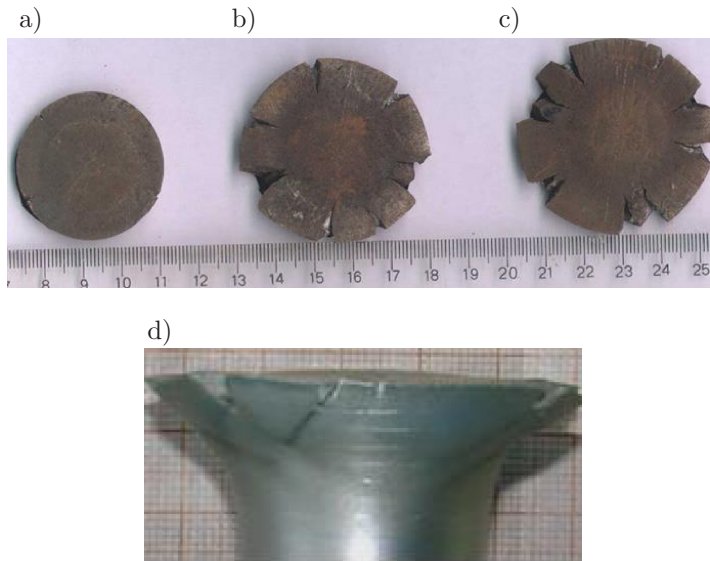


FIG. 15. Top view (a, b, c) and side view (d) failure of specimen:  
 a) 217 m/s, b) 290 m/s, c) 319 m/s, d) 319 m/s.

consistent with the experimental observation. The failure in the specimen was intensified, and the spiral shear failure in the specimen lateral face was observed, while the impact velocity increased to 319 m/s. Various failure characteristics of Taylor impact experiments were obtained. Although there is some uncertainty, it appears that the obtained parameters can describe the fracture behaviour of 45 steel under high speed deformation. When the impact velocity was further increased, the failure appeared at the end of the impact end, and the specimen head broke.

The deformation and failure process of 45 steel Taylor impact specimen for the case of impact velocity of 310 m/s is given in Fig. 16. From this figure it can be seen that, at the time of 60  $\mu$ s after the impact, numerous element failures appeared at the edge of the impact end, and this caused the formation of crack. As the specimen deformation further increased, more and more elements failed, which led to the further development of the crack. Although initially a large number of cracks appeared, eventually only some of the cracks grew; as the length of cracks grew to a certain stage, at the time of 140  $\mu$ s cracks began to bifurcate a, and then they grew spirally.

The characteristics of the specimen damage and fracture can be described with stress state triaxiality histories. The failure strain of material was dominated by the stress state triaxiality, the fracture strains increased markedly with stress triaxiality. At the central part of the specimen, material was always sub-



FIG. 16. Deformation failure process of 45 steel Taylor impact specimen (310 m/s).

jected to compressive loading, and at the edge of specimen, material was under the stress state of circumferential tensile. Thus, failure would first occur at the specimen edge.

## 5. SUMMARY

In this study, the deformation and fracture characteristics of 45 steel were simulated numerically during Taylor impact tests with material model parameters calibrated by various material properties experiments.

The specimen deformation of Taylor impact obtained with two-dimensional axisymmetric numerical simulation was consistent with experimental observation. Two of the simulation results: the loading characteristics and the temperature rise were discussed. By analysing stress state triaxiality histories, it can

be concluded that material failure may first occur at the edge of the specimen, despite the fact that the strain at the centre part is much larger than that at the edge.

Next, the specimen failure under Taylor impact was simulated with 3D solid model. Various failure characteristics observed in the Taylor impact experiments were presented.

#### ACKNOWLEDGMENT

The authors would like to acknowledge the financial support of China National Natural Science Foundation (Grant no. 11572299, 11472257 and 10302211) and the key subject “Computational Solid Mechanics” of China Academy of Engineering Physics (CAEP).

#### REFERENCES

1. JOHNSON G.R., COOK W.H., *A constitutive model and data for metals subjected to large strains, high strain rates and high temperatures*, Proceedings of the 7th International Symposium on Ballistics, Hague, Netherlands, 19–21 April, 1983, pp. 541–547.
2. FOSTER J.C. JR., GILMORE M., WILSON L.L., *The use of the Taylor test in exploring and validating the large-strain, high-strain-rate constitutive response of materials*, [in:] Shock Compression of Condensed Matter – 2001, Furnish M.D., Thadhani N.N., Horie Y. [Eds.], American Institute of Physics, New York, 2002, pp. 1318–1322.
3. ROHR L., NAHME H., THOMA K., *A modified Taylor-test in combination with numerical simulations – a new approach for the determination of model parameters under dynamic loads*, Journal de Physique IV France, **110**: 513–518, 2003.
4. BRÜNING M., DRIEMEIER L., *Numerical simulation of Taylor impact tests*, International Journal of Plasticity, **23**(12): 1979–2003, 2007.
5. REVEL-BAUDARD B., CAZACU O., FLATER P., KLEISER G., *Plastic deformation of high-purity  $\alpha$ -titanium: model development and validation using the Taylor cylinder impact test*, Mechanics of Materials, **80** (Part B): 264–275, 2015.
6. JOHNSON G.R., HOLMQUIST T.J., *Evaluation of cylinder-impact test data for constitutive model constants*, Journal of Applied Physics, **64**(8): 3901–3910, 1988.
7. HERNANDEZ C., MARANON A., ASHCROFT I.A., CASAS-RODRIGUEZ J.P., *A computational determination of the Cowper–Symonds parameters from a single Taylor test*, Applied Mathematical Modelling, **37**(7): 4698–4708, 2013.
8. NUSSBAUM J., FADERL N., *Evaluation of strength model parameters from Taylor impact tests*, Procedia Engineering, **10**: 3453–3458, 2011.
9. PAPIRNO R.P., MESCALL J.F., HANSON A.M., *Beyond the Taylor test to fracture*, Proceedings of the Army Symposium on Solid Mechanics, AMMRC Monograph MS 80-4, Army Materials and Mechanics Research Center, Watertown, Mass., pp. 367–385, 1980.
10. GRADY D.E., KIPP M.E., *Fragmentation of solids under dynamic loading*, [in:] Wierzbicki T., Jones N. [Eds.], Structural Failure, John Wiley & Sons, New York, pp. 1–40, 1989.

11. WOODWARD R.L., O'DONNELL R.G., FLOCKHART C.J., *Failure mechanisms in impacting penetrators*. Journal of Materials Science, **27**(23): 6411–6416, 1992.
12. REN Y., TAN C.W., ZHANG J., WANG F.C., *Dynamic fracture of Ti-6Al-4V alloy in Taylor impact test*, Transactions of Nonferrous Metals Society of China, **21**(2): 223–235, 2011.
13. XIAO X., ZHANG W., WEI G., MU Z., GUO Z., *Experimental and numerical investigation on the deformation and failure behaviour in the Taylor test*, Materials and Design, **32**(5): 2663–2674, 2011.
14. RAKVÅG K.G., BØRVIK T., WESTERMANN I., HOPPERSTAD O.S., *An experimental study on the deformation and fracture modes of steel projectiles during impact*, Materials and Design, **51**: 242–256, 2013.
15. MOĆKO W., JANISZEWSKI J., RADZIEJEWSKA J., GRAZKA M., *Analysis of deformation history and damage initiation for 6082-T6 aluminium alloy loaded at classic and symmetric Taylor impact test conditions*, International Journal of Impact Engineering, **75**: 203–213, 2015.
16. TENG X., WIERZBICKI T., HIERMAIER S., ROHR I., *Numerical prediction of fracture in the Taylor test*, International Journal of Solids and Structures, **42**(9–10): 2929–2948, 2005.
17. CHEN X.W., CHEN G., ZHANG F.J., *Deformation and failure modes of soft steel projectiles impacting harder steel targets at increasing velocity*, Experimental Mechanics, **48**(3): 335–354, 2008.
18. RAKVÅG K.G., BØRVIK T., HOPPERSTAD O.S., *A numerical study on the deformation and fracture modes of steel projectiles during Taylor bar impact tests*, International Journal of Solids and Structures, **51**(3–4): 808–821, 2014.
19. JOHNSON G.R., COOK W.H., *Fracture characteristics of three metals subjected to various strains, strain rates, temperatures, and pressures*, Engineering Fracture Mechanics, **21**(1): 31–48, 1985.
20. CHEN G., CHEN Z.F., TAO J.L., NIU W., ZHANG Q.P., HUANG X.C., *Investigation and validation on plastic constitutive parameters of 45 steel [in Chinese]*, Explosion and Shock Waves, **25**(5): 451–456, 2005.
21. CHEN G., CHEN Z.F., XU W.F., CHEN Y.M., HUANG X.C., *Investigation on the JC ductile fracture parameters of 45 steel [in Chinese]*, Explosion and Shock Waves, **27**(2): 131–135, 2007.

*Received July 21, 2015; accepted version January 29, 2016.*

---